

PERFORMANCE COMPARISONS BETWEEN CONVENTIONAL AND HAIRPIN WINDING CONFIGURATIONS OF V-SHAPED IPMSM

Vuong Dang QUOC^{1,2} , Dinh Bui MINH^{1,2}, Hung Bui DUC^{1,2}, Phi Do CHI^{3,*}

¹Laboratory of High performance electric machines (HiPems)

²School of Electrical and Electronic Engineering, Hanoi University of Science and Technology, No.1, Dai Co Viet Street, Hai Ba Trung District, Hanoi, Viet Nam

³Electrical-Electronic Engineering, Cao Thang Technical College, Viet Nam

vuong.dangquoc@hust.edu.vn, dinh.buiminh@hust.edu.vn, hung.buiduc@hust.edu.vn,
dochiphi@caothang.edu.vn

*Corresponding author: Phi Do CHI; dochiphi@caothang.edu.vn

DOI: 10.15598/aece.v23i2.240904

Article history: Received Sep 03, 2024; Revised Oct 05, 2024; Accepted Nov 29, 2024; Published Jun 30, 2025.
This is an open access article under the BY-CC license.

Abstract. Interior permanent magnet synchronous motors (IPMSMs) have been used extensively in the transportation, industrial, medical, and military fields recently because of their many benefits, including high power density, high torque, and high operational economy. However, current studies have mainly focused on using traditional windings for these motors, neglecting the potential improvements in motor performance that could be achieved with different winding types. Therefore, it is crucial to evaluate the performance of these motors when using different winding structures. This paper presents a combination of analytical technique and finite element method to compare the electromagnetic parameters (back electromotive force (EMF), output power and torque, and temperature rise) of IPMSMs with conventional and hairpin winding configurations. The validated method is then applied to a practical V-shape IPMSM with conventional and hairpin winding configurations.

Keywords

Interior permanent magnet synchronous motor (IPMSM), V-shape rotor configuration, hairpin winding type, analytical model, finite element method.

1. Introduction

Internal Permanent Magnet Synchronous Motors (IPMSMs) have been widely used in the transportation, industrial, medical, and military sectors due to their numerous advantages, such as high torque, high power density, and high operational efficiency. However, most prior research has focused on IPMSMs with conventional windings [1–5]. This is a partial assessment of the potential improvements in motor performance that could be achieved by employing different types of windings. Therefore, it is crucial to evaluate how well a motor performs when using various winding configurations. In reference [1], the IPMSM with conventional winding type was presented. In this study, every component of the magnetic flux channels was included in the model, particularly the leakage flux paths surrounding the permanent magnets (PMs). The results showed that the width of the iron bridge and the level of iron saturation significantly influenced the distribution of the magnetic field inside the motor. The validity of the analytical model was confirmed by the numerical results. In reference [2], an enhanced analytical technique for computing the cogging torque and magnetic field in surface-mounted PMSMs (SPMSMs) that takes into account any eccentric rotor form was presented. Based on the subdomain model, the superposition concept of the vector potential, and the surface-current approach of the per-

manent magnet (PM), the expected magnetic field in the surface-mounted PM machines was discussed. In reference [3], the electromagnetic performance of the IPMSM with a $\nabla + U$ PM configuration was compared to the normal $V + \nabla$ shape for EV applications. For this structure, the paper used the finite element analysis (FEA) to maximize basic air-gap flux density while minimizing total harmonic distortion (THD). In reference [4] a novel method was developed for an asymmetrical V-type rotor configuration to reduce the cogging torque and torque ripple. The torque ripple and cogging torque were also compared to those of the baseline model. The results demonstrate that adopting the proposed rotor considerably reduces both the cogging torque and torque ripple. In reference [5], this research proposed an asymmetric rotor IPMSM with strong torque performance and great demagnetization prevention capacity. Two factors make up this paper's main contribution. To increase the torque density and ability to prevent demagnetization, a unique asymmetric rotor with a shifted magnet axis is presented. In reference [6], the fractional-slot concentrated-winding (FSCW) PMSM was thoroughly examined for its advantages and disadvantages. This paper discussed the theory and design of FSCW PMSMs. The comparative different types of machines, fault-tolerance rotor losses, parasitic effects, and IPMSM and SPMSM were also performed. In reference [7], the authors described three-phase machine designs with focused windings. The first section shows structures with a regular slot distribution and analyzes their performance, as well as a method for finding the windings. In reference [8], the paper explained how to develop high-performance permanent magnet machines with concentrated windings. In reference [9], a consequent-pole (CP) PM machine with an asymmetric magnetic pole (AMP) structure was proposed to produce decreased torque ripple and unipolar leakage flux. In reference [10], a study examined two configurations of twin three-phase windings based on the Toyota Prius's IPMSM 2010. It was discovered that in the constant torque range, a winding structure with single-layer full-pitched (SF) windings can improve average torque while decreasing torque ripple. The electromagnetic properties of the two winding topologies were compared, with one winding set activated and the other open-circuited.

As presented above, up to now, there have been many studies on improving the electromagnetic parameters of IPMSM and SPMSM using different methods. However, comparing and evaluating the electromagnetic parameters of IPMSM with a V-shape rotor type when using conventional windings and Hairpin windings has not been presented before. In this research, a coupling of analytical MATLAB software and the FEA is proposed for IPMSM with conventional and hairpin winding configurations. Firstly, an analytical MATLAB software is first developed to define the ini-

tial/required parameters of the proposed motor. Next, the FEA is presented to simulate and evaluate electromagnetic parameters, such as the back electromotive force (EMF), output power, torque ripple, cogging torque, and temperature rise of the IPMSM. The obtained results will give the electromagnetic improvements of hairpin windings compared to conventional windings. The validated methods are applied to the practical IPMSM with a V-shape rotor configuration.

2. Analytical Background

The expression for electromagnetic torque (T_e) has been calculated based on the stator and rotor diameter, power inverter voltage, and currents:

$$T_e = \frac{\pi}{2} D^2 L_{stk} \sigma, \quad (1)$$

where L_{stk} is the stack length, D is the rotor diameter, and $\sigma = L/D$ is defined for the inner rotor between 0.8 and 1.25. When the rotor is spun, the finite element grid automatically adjusts, and torque prediction is performed for any stator-rotor relative position. To obtain acceptable precision while avoiding errors brought on by element distortion, the impact of the mesh has been studied. The motor symmetry allows for the simulation of only one pole.

The equations below express the steady-state stator voltage in the d - q rotating reference frame [11–13]:

$$v_d = R i_d - \omega L_d i_q, \quad (2)$$

$$v_q = R i_q + \omega L_d i_d + \lambda_m \omega, \quad (3)$$

$$\lambda_d = L_d i_d + \lambda_m, \quad \lambda_q = L_q i_q + \lambda_m, \quad (4)$$

where R is the winding resistance per phase, and L_d , L_q are the direct and quadrature axis inductances, λ_m is the linkage flux of PM along the d - and q - axes, ω is the electrical speed, and v_d , i_d , v_q , i_q are the direct and quadrature axis components of the armature current and terminal voltage, respectively. The well-known term " T_e " is defined as [14], [15].

$$T_e = \frac{3}{2} p [\phi_m i_d + (L_d - L_q) i_d i_q] \quad (5)$$

According to mathematical terms, the cogging torque (T_{cog}) is defined as follows and is classified as a component of the magnetic torque [15]:

$$T_{cog} = -\frac{1}{2} \phi_m^2 \frac{dR}{d\theta} \quad (6)$$

where θ is the rotor angle, R is the total reluctance through the flux channels, and ϕ_m is the magnet flux crossing the air gap. The cogging torque (T_{cog}) will be zero if the reluctance R does not change while the

rotor turns. According to this theory, by adjusting the V-shaped rotor’s structural variables that influence the reluctance R , the T_{cog} can be increased. When it comes to torque ripple (T_{ripple}), a small mismatch between the back EMF of machine and the current often causes it. It is important to achieve a sinusoidal back EMF waveform and sinusoidal air-gap flux density because the windings of the IPMSM are powered by three-phase sinusoidal currents. Therefore, it is crucial to consider the air-gap flux density B_g , which is represented as follows [16, 17]

$$B_g = \frac{\phi_g}{A_g} = \mu_0 \frac{F_g}{l_g} \tag{7}$$

In this equation, l_g represents the air gap equivalent length, A_g represents the air gap’s cross-sectional area, μ_0 represents vacuum permeability, and F_g represents the air gap magnetomotive force. Since the electrical angle “ θ ” ranges between -90° and 90° , the equation (7) can be written as a periodic function.

$$B_g = B_{max} \cos \theta = \mu_0 \frac{F_g}{l_g(\theta)} \tag{8}$$

where B_{max} is the maximum air-gap flux density. As shown in equation (8), a sinusoidal air-gap flux density distribution can be obtained a maximum value at the d-axis point by setting θ equal to zero. Furthermore, in the perfect scenario, the air-gap flux density changes sinusoidally as θ changes. Subsequently, the air-gap equivalent length l_g depends on the θ . The use of V-shaped PM rotors with varying air-gap equivalent lengths, it is an efficient way to reduce both the T_{cog} and T_{ripple} . This is accomplished by creating a sinusoidal air-gap flux density waveform and the T_{cog} . Thus, the T_{ripple} is defined as [18–20]:

$$T_{ripple} = -\frac{T_{max} - T_{min}}{T_{average}} 100\% \tag{9}$$

where T_{max} is the maximum torque, T_{min} is the minimum torque, and $T_{average}$ is the average torque.

3. Finite Element Analysis

In this part, the FEA is applied for a double V-shaped (VV-shaped) IPMSM with the hairpin winding configuration to analyze electromagnetic parameters (magnetic flux field, back EMF, output power, output torque, cogging torque and temperature rise). The input parameters of the proposed machine are given fully in Table 1. The stator and rotor laminations of the motor with model Airways U5 Premium 2020 are pointed out in Figure 1.

Tab. 1: Input parameters of VV-shaped IPMSM with hairpin winding configuration.

No	Parameters	Value	Unit
1	Input power	150	kW
2	Hairpin Winding	15.729	kg
3	Core of rotor	7.542	kg
4	Permanent magnet	1.644	kg
5	Shaft	1.43	kg
6	End cap	1.44	kg
7	Voltage	350	VDC
8	Number of pole pair	8	pole
9	Slots of stator	48	slots
10	Diameter of shaft	52	mm
11	Outer diameter of rotor	147.6	mm
12	Inner diameter of stator	149	mm
13	Length of air gap	0.7	mm
14	Stack length of stator	116	mm
15	Stack length of rotor	116.6	mm

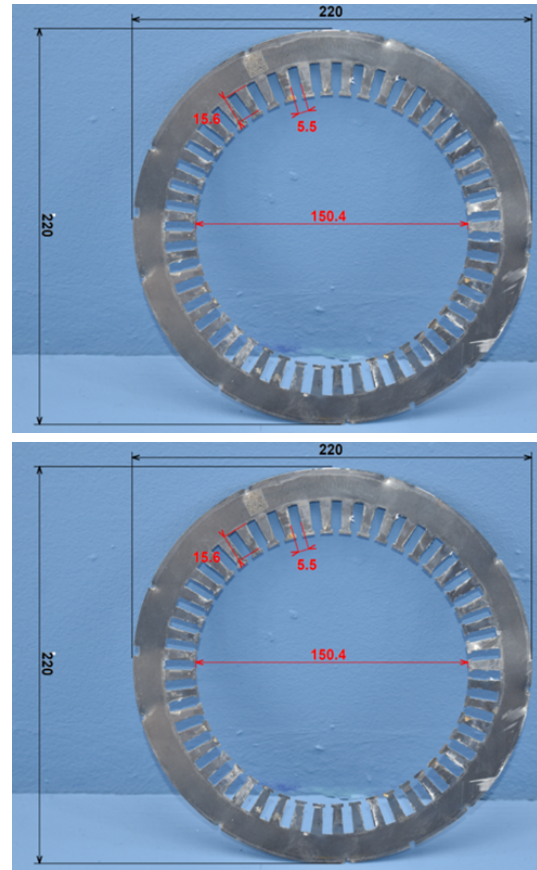


Fig. 1: Stator (top) and rotor (bottom) laminations of motor (Model: Airways U5 Premium 2020).

The modeling of the proposed motor with the VV-shaped IPMSM with $p = 4$ is presented in Figure 2. The detailed hairpin winding structure is pointed out in Figure 3. The distribution of magnetic flux density is shown in Figure 4. It can be seen that the magnetic

flux density near the barriers is the highest, with a value of 2.103 T compared to other regions. Because the magnetic flux density due to the current in the armature windings, was significantly diminished based on the presence of the bridge space from the flux barrier and also the angle between two barriers. The indication of barrier angle has been still a challenge for researchers and designers, so far.

It is clear that within the speed range of 1500 rpm to 5000 rpm, the hairpin winding has a higher capacity than that of the traditional winding. Specifically, at a speed of 5000 rpm, the power output is 195 kW for hairpin winding and 180 kW for the conventional winding. When the speed is greater than 6000 rpm, the power of the two cases is almost unchanged.

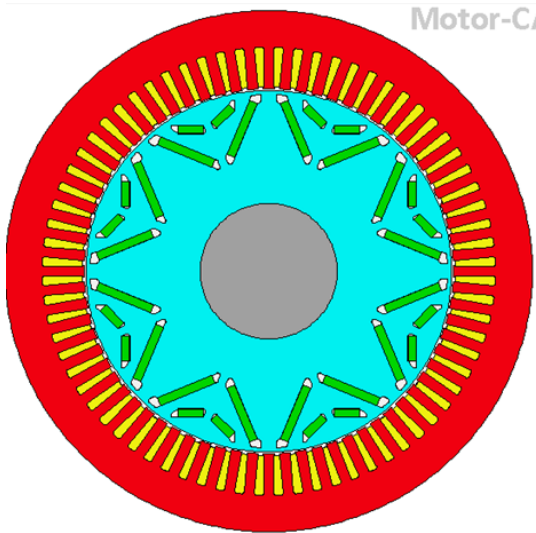


Fig. 2: Model of the proposed motor with VV-shaped IPMSM.

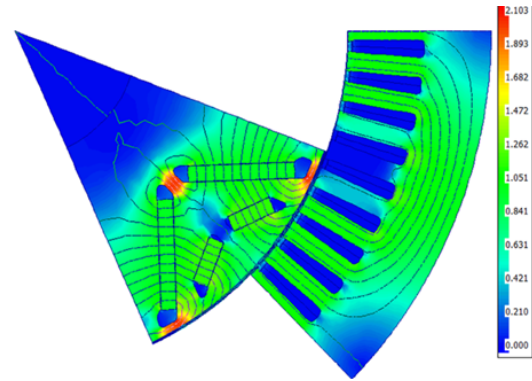


Fig. 4: Distribution of magnetic flux density in rotor and stator.

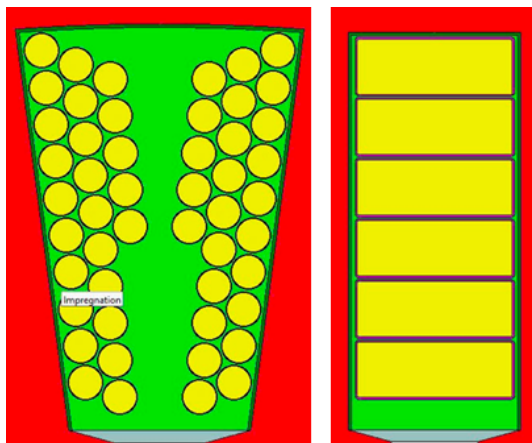


Fig. 3: From the left to right sides: model of conventional and hairpin winding configuration.

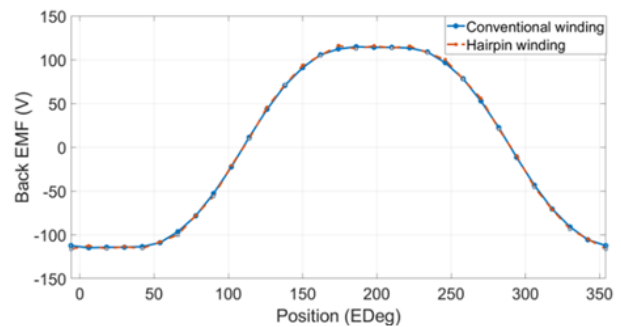


Fig. 5: Back EMF waveform of conventional and hairpin winding configurations.

Figure 5 shows the distribution the back EMF waveforms of conventional and hairpin winding configurations, which are closer to sinusoidal wave forms. It can be visualized that the amplitude of the back EMF waveform for both cases is quite similar, i.e., 113.5 V and 114.9 V for the convention hairpin windings, respectively.

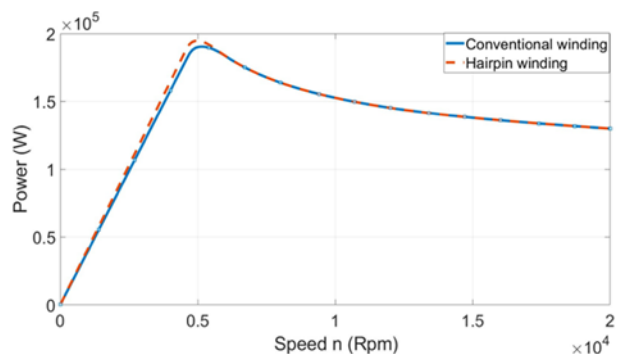


Fig. 6: Power comparison of conventional and hairpin winding configurations.

The comparison of power between conventional and hairpin winding configurations is shown in Figure 6.

Figure 7 illustrates the comparison of electromagnetic torque between conventional and hairpin winding configurations. Similarly to the power output, in

the speed range from 0 rpm to 5000 rpm, the electromagnetic torque of the hairpin winding is greater than that of the conventional winding. At the speed of 5000 rpm, the torque is 360 N.m for the conventional winding and 375 N.m for the hairpin winding. In the same way, at the greater speed of 5000 rpm, the electromagnetic torque of the two cases are quite stable.

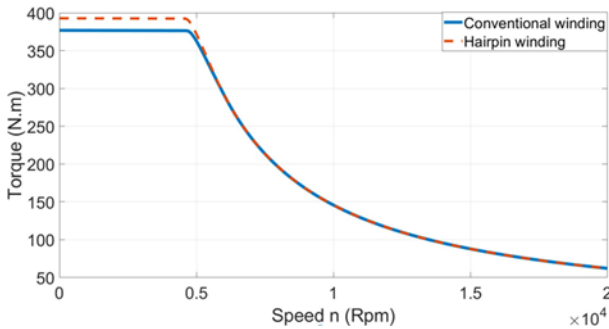


Fig. 7: Electromagnetic torque comparison of conventional and hairpin winding configurations.

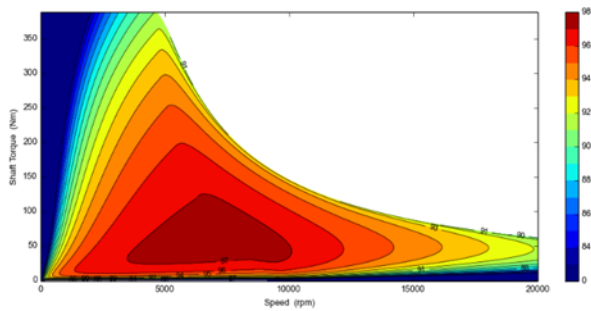


Fig. 8: Torque and efficiency of hairpin winding configuration.

Another important results on the torque and efficiency of the hairpin winding is presented via the map shown in Figure 8. It shows that at a range of speed from 5000 rpm to 6000 rpm, the efficiency can reach approximately 95%. This also means that the high efficiency can reach at low speed and low torque. Figure 9 illustrates the temperature rise for both conventional and hairpin winding configurations. The temperature at the center of the conventional winding is higher than that of the hairpin winding, with a range from 30°C to 60°C. The maximum temperature of 110.70C is near to the connection of the winding, while in the rotor the temperature is about 75.90C. The minimum temperature is on the shaft of motor. Additionally, a comparison of the electromagnetic properties of conventional and hairpin windings, showing that the electromagnetic power, total losses, and efficiency of the hairpin winding are higher than those of the traditional winding.

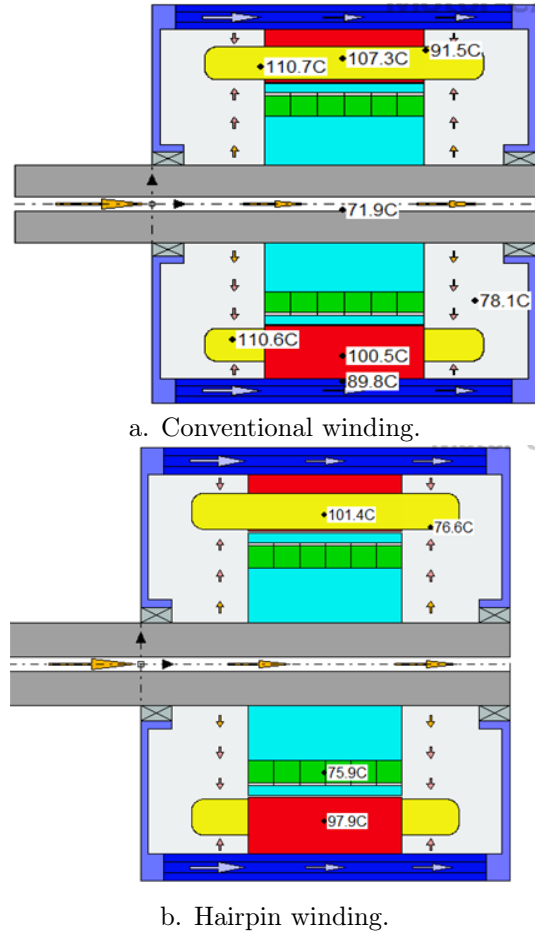


Fig. 9: Temperature rise of conventional (a) and hairpin winding (b) configurations.

4. Conclusion

In this research, both analytical model and FEA has been proposed to compare two types of windings (conventional and hairpin windings) of the VV shapes-IPMSMs. The obtained results on the back EMF, electromagnetic torque, output power, cogging torque, torque ripple, efficiency and temperature rise have pointed out the advantages of using the hairpin winding compared to the conventional winding as shown in Table 2. However, hairpin winding also has some disadvantages compared to regular windings, that is, the T_{cog} and T_{ripple} of hairpin winding are larger than that of conventional winding. Finally, considering the advantages of the hairpin winding technology, novel design concepts for improving motor performance are presented. The obtained solutions allow to reach the benefits of the hairpin winding technology while simultaneously resolving its limitations.

Tab. 2: Comparison of electromagnetic parameters between the conventional and hairpin windings.

Parameters	Hairpin	Conventional	Nm
Maximum torque	348.57	344.28	Nm
Torque ripple [%]	7.4182	6.0042	%
Cogging torque	7.766	4.0963	Nm
Speed	5677	5975	rpm
Electromagnetic power	150040	148206	Watts
Input Power	155654	141757	Watts
Output Power	152340	139927	Watts
Total losses (on load)	1827.3	1830.1	Watts
Efficiency	98.043	95.617	%
Shaft Torque	355.41	345.64	Nm

Author Contributions

V.D.Q. and P.D.C. developed the analytical model and finite element method for the conventional and Hairpin winding configurations of V-Shaped IPMSM. D.B.M. performed the simulation of the proposed motor. H.B.D. checked and analysed results of the manuscript. All authors contributed to the final version of the manuscript.

References

- [1] HWANG, C.-C., Y. H. CHO. Effects of leakage flux on magnetic fields of interior permanent magnet synchronous motors. *IEEE Transactions on Magnetics*. 2001, vol. 37, no. 4, pp. 3021-3024. DOI: 10.1109/20.947055.
- [2] ZHOU, Y., H. LI, G. MENG, S. ZHOU, Q. CAO. Analytical Calculation of Magnetic Field and Cogging Torque in Surface-Mounted Permanent-Magnet Machines Accounting for Any Eccentric Rotor Shape. *IEEE Transactions on Industrial Electronics*. 2015, vol. 62, no. 6, pp. 3438-3447. DOI: 10.1109/TIE.2014.2369458.
- [3] HU, Y., S. ZHU, C. LIU, K. WANG. Electromagnetic Performance Analysis of Interior PM Machines for Electric Vehicle Applications. *IEEE Transactions on Energy Conversion*. 2018, vol. 33, no. 1, pp. 199-208. DOI: 10.1109/TEC.2017.2728689.
- [4] REN, W., Q. XU, Q. LI, L. ZHOU. Reduction of Cogging Torque and Torque Ripple in Interior PM Machines With Asymmetrical V-Type Rotor Design. *IEEE Transactions on Magnetics*. 2016, vol. 52, no. 7, pp. 1-5. DOI: 10.1109/TMAG.2016.2530840.
- [5] LING, D., et al. Design and Optimization of an Asymmetric Rotor IPM Motor with High Demagnetization Prevention Capability and Robust Torque Performance. *Energies*. 2023, vol. 16, no. 9. DOI: 10.3390/en16093635.
- [6] EL-REFAIE, A. M. Fractional-Slot Concentrated-Windings Synchronous Permanent Magnet Machines: Opportunities and Challenges. *IEEE Transactions on Industrial Electronics*. 2010, vol. 57, no. 1, pp. 107-121. DOI: 10.1109/TIE.2009.2030211.
- [7] CROS, J., P. VIAROUGE. Synthesis of high performance PM motors with concentrated windings. *IEEE Transactions on Energy Conversion*. 2002, vol. 17, no. 2, pp. 248-253. DOI: 10.1109/TEC.2002.1009476.
- [8] MAGNUSSEN, F., C. SADARANGANI. Winding factors and Joule losses of permanent magnet machines with concentrated windings. *IEEE International Electric Machines and Drives Conference, 2003. IEMDC'03., Madison, WI, USA*. 2003, pp. 333-339 vol.1. DOI: 10.1109/IEMDC.2003.1211284.
- [9] LI, F., K. WANG, J. LI, H. Y. SUN. Electromagnetic Performance Analysis of Consequent-Pole PM Machine With Asymmetric Magnetic Pole. *IEEE Transactions on Magnetics*. 2019, vol. 55, no. 6, pp. 1-5. DOI: 10.1109/TMAG.2019.2904948.
- [10] WANG, S., et al. Comparison of Different Winding Configurations for Dual Three-Phase Interior PM Machines in Electric Vehicles. *World Electric Vehicle Journal*. 2022, vol. 13, no. 3. DOI: 10.3390/wevj13030051.
- [11] ARZILLO, A., et al. Challenges and Future opportunities of Hairpin Technologies. *2020 IEEE 29th International Symposium on Industrial Electronics (ISIE), Delft, Netherlands*. 2020, pp. 277-282. DOI: 10.1109/ISIE45063.2020.9152417.
- [12] BIANCHI, N., G. BERARDI. Analytical Approach to Design Hairpin Windings in High Performance Electric Vehicle Motors. *2018 IEEE*

- Energy Conversion Congress and Exposition (ECCE), Portland, OR, USA.* 2018, pp. 4398-4405. DOI: 10.1109/ECCE.2018.8558383.
- [13] MARJIUAN, M., I. MARTINEZ, F. GARRAMIOLA. A comparison between continuous and hair-pin windings for electric traction drives. *2023 13th International Electric Drives Production Conference (EDPC), Regensburg, Germany.* 2023, pp. 1-8. DOI: 10.1109/EDPC60603.2023.10372165.
- [14] LIU, X., H. CHEN, J. ZHAO, A. BELAH-CEN. Research on the Performances and Parameters of Interior PMSM Used for Electric Vehicles. *IEEE Transactions on Industrial Electronics.* 2016, vol. 63, no. 6, pp. 3533-3545. DOI: 10.1109/TIE.2016.2524415.
- [15] PENG, G., et al. Improved V-shaped interior permanent magnet rotor topology with inward-extended bridges for reduced torque ripple. *IET Electric Power Applications.* 2020, vol. 14, iss. 12, pp. 2404-2411. DOI: 10.1049/iet-epa.2019.0850.
- [16] HUYNH, T. A., M.-F. HSIEH. Performance Analysis of Permanent Magnet Motors for Electric Vehicles (EV) Traction Considering Driving Cycles. *Energies.* 2018, vol. 11, no. 6. DOI: 10.3390/en11061385.
- [17] LIU, H., H. ZHANG, J. ZHANG. PM Design of IPMSM using Parameterized Finite Element Model. *Indonesian Journal of Electrical Engineering and Computer Science.* 2013, vol. 11, no. 12, pp. 7072-7080. DOI: 10.11591/telkomnika.v11i12.3745.
- [18] CHU, W. Q., Z. Q. ZHU. Investigation of Torque Ripples in Permanent Magnet Synchronous Machines With Skewing. *IEEE Transactions on Magnetics.* 2013, vol. 49, no. 3, pp. 1211-1220. DOI: 10.1109/TMAG.2012.2225069.
- [19] DANG, V., T. TRUONG, T. VU, H. THANH. Performance Comparison Of A Six Phase Surface-Mounted Pmsm With Inner And Outer Rotor Types For High Torque Applications. *Advances in Electrical and Electronic Engineering.* 2024, vol. 22, no. 2, pp. 172-183. DOI: 10.15598/aece.v22i2.5536.
- [20] ZHOU, Y., H. LI, G. MENG, S. ZHOU, Q. CAO. Analytical Calculation of Magnetic Field and Cogging Torque in Surface-Mounted Permanent-Magnet Machines Accounting for Any Eccentric Rotor Shape. *IEEE Transactions on Industrial Electronics.* 2015, vol. 62, no. 6, pp. 3438-3447. DOI: 10.1109/TIE.2014.2369458.